Design of Drilling and Riveting Multi-functional End Effector for CFRP and Aluminum Components in Robotic Aircraft Assembly

Zhang Lin[1*], *Tian Wei*[1], *Li Dawei*[1], *Hong Peng*[1], *Li Zhenyu*[1], *Zhou Weixue*[1], *Liao Wenhe*[1,2]

1. College of Mechanical & Electrical Engineering, Nanjing University of Aeronautics and Astronautics, Nanjing 210016, P. R. China;

2. School of Mechanical Engineering, Nanjing University of Science and Technology, Nanjing 210094, P. R. China

(Received 31 December 2015; revised 17 June 2016; accepted 22 June 2016)

Abstract: To fulfill the demands for higher quality, efficiency and flexibility in aviation industry, a multi-functional end effector is designed to automate the drilling and riveting processes in assembling carbon fiber reinforced polymer (CFRP) and aluminum components for a robotic aircraft assembly system. To meet the specific functional requirements for blind rivet installation on CFRP and aluminum materials, additional modules are incorporated on the end effector aside of the basic processing modules for drilling. And all of these processing modules allow for a one-step-drilling-countersinking process, hole inspection, automatic rivet feed, rivet geometry check, sealant application, rivet insertion and installation. Besides, to guarantee the better quality of the hole drilled and joints riveted, several online detection and adjustment measures are applied to this end effector, including the reference detection and perpendicular calibration, which could effectively ensure the positioning precision and perpendicular accuracy as demanded. Finally, the test result shows that this end effector is capable of producing each hole to a positioning precision within ± 0.5 mm, a perpendicular accuracy within 0.3°, a diameter tolerance of H8, and a countersink depth tolerance of ± 0.01 mm. Moreover, it could drill and rivet up to three joints per minute, with acceptable shearing and tensile strength.

Key words: robotic aircraft assembly; CFRP and aluminum components; automatic drilling and riveting; multi-functional end effector; online detection and adjustment

CLC number: V261.97 **Document code**: A **Article ID**: 1005-1120(2018)03-0529-10

0 Introduction

Recently, the requirements of the aircraft assembly technology for higher quality, efficiency and flexibility have been put forward by the aviation industry, which also demands a higher adaptability to the specific production characteristic of small quantity with large variety, and the off-the-shelf industrial robots, with their increasing maturity, may make these urgent requirements fulfilled. Since robots offer many distinct advantages, such as flexibility, cost-effectiveness, minimal installing disruption and large working volume, their implementations have become a distinguished characteristic in aviation industry for drilling, riveting, painting and inspection, etc[1-5]. And in the meantime, because of its high specific strength and excellent mechanical properties, the extensive application of composites has become another distinguished characteristic in the new generation of aircraft.

Usually, the assembly of carbon fiber reinforced polymer (CFRP) and aluminum components is mainly accomplished by drilling and blind rivet installation, the quality of which will immediately influence the performance and longevity of

* Corresponding author, E-mail address: zhanglin05@nuaa.edu.cn.

How to cite this article: Zhang Lin, Tian Wei, Li Dawei, et al. Design of drilling and riveting multi-functional end effector for CFRP and aluminum components in robotic aircraft assembly[J]. Trans. Nanjing Univ. Aero. Astro., 2018,35(3): 529-538.

http://dx.doi.org/10.16356/j.1005-1120.2018.03.529

the aircraft[6]. Since a high precision and quality consistency could not be easily maintained through the traditional manual implements, the automatic drilling and riveting system based on robot has become an extensive tendency in place of hand operations in aviation industry[7]. As an inextricable constituent of a typical robotic automatic drilling and riveting system, the multifunctional end effector usually works as the final processing equipment, the design of which is the key to fulfill the different processing tasks. A one-sided cell end effector system, as well as its upgraded version of robotic trailing edge flap drilling system, both are developed by Electroimpact Company, the end effectors of which could automatically drill, countersink, and measure hole's diameter in material stack combinations of aluminum, titanium, and composite on an aircraft trailing edge flaps[8-9]. A new 787 robot system, developed by Hawker de Havilland-a Division of Boeing, is built for assembling several composite components of the Boeing 787 Dreamliner, and its end effector is capable of drilling, countersinking on both upper and lower skins for each assembly[10]. Another robot assembly cell is developed by BROETJE-Automation, whose end effector is capable of drilling and installing solid rivet in cargo door structures of a single aisle aircraft at EUROCOPTER in Germany[11]. All in all, these robotic aircraft assembly systems mentioned above have been proved highly successful through years of practical applications.

Compared to the robotic automatic assembly technology developed abroad, the domestic aircraft assembly technology still falls far behind, and the researches, which usually focus on drilling aluminum materials, are mainly conducted by a few universities and research institutions. A robot automatic drilling system is developed by Zhejiang University for drilling and countersinking on the aluminum laminated stacks[12]. Its end effector could drill up to six holes per minute with a diameter precision of H9, however it lacks the hole inspection unit and the processing module for rivet installation, so the riveting process must be carried out manually afterward, which will partly compromise the final efficiency and quality of the production. Recently, Wuhan Ship Development & Design Institute has developed a traveling robot automatic drilling and riveting system. The robot is innovatively mounted on a mobile vehicle to enlarge the working envelop, and the end effector could successfully drill, countersink and install blind rivets on the aluminum stacks[13]. However, the end effector of this system has to execute the drilling process and the riveting process separately, because of the exchange of each processing module. Since it could not achieve a "one-up" assembly, the final assembly efficiency is only increased limitedly.

To automate the drilling and riveting processes for assembling CFRP and aluminum components of an aircraft, such as rudders and vertical fins, a one-sided robotic automatic system has been developed, the end effector of which could conduct the one-step-drilling-countersinking process and blind rivet installation successively in material stack combinations of aluminum and CFRP. To achieve this one-up assembly goal discussed above, additional processing modules have been incorporated on the end effector for facilitating the final riveting process, such like the rivet reception and geometry check module, sealant application module, etc. Besides, to better guarantee the quality of the hole drilled and joints riveted, such like the positioning precision and the perpendicular accuracy, several online detection and adjustment measures have also been applied to this end effector. In the field application, this end effector is capable of producing each hole and joint, with a better precision and quality than traditional methods.

1 Schematic Design of End Effector

The assembly of CFRP and aluminum components of an aircraft, such as rudders and vertical fins, usually needs to drill, countersink on the CFRP and aluminum laminated materials. Since CFRP materials could not allow interface-riveting, which will cause the defection of the materi-

als, such like delamination, fiber break etc., these CFRP and aluminum laminated materials demand us to install blind rivet, and sometimes have special requirement for sealant application. Usually a typical drilling and riveting circle in assembling aircraft CFRP and aluminum components follows the following procedures: clamp, drill, countersink, rivet selection, rivet check, sealant application, blind rivet insertion and installation. For one-up assembly, all these processes must be accurate, repeatable, and automatically. And there must be minimal exit burrs, fiber breakout, delamination, and inter-laminar contamination to preclude the need to deburr and clean. To further achieve these goals, we should select specific drills and processing parameters, such like spindle rotary speed, feed speed and clamping force, for each processing situations, according to the studied processing mechanisms of different materials, such like the burr formation mechanism for single or laminated aluminum and CFRP materials, fiber break mechanism and delamination mechanism for CFRP materials. This paper mainly focuses on the designs of the end effector, so these studies will not be illustrated in detail. But it should be noted that, the required specific processing parameters must be accurately carried out by the elaborately designed functional modules on the end effector, such like the pressure foot and the drilling & countersinking module. Besides, each hole must be inspected for correct diameter, countersink depth and actual stack thickness. In addition, each blind rivet must be pre-checked for the proper diameter and grip length. Based on analysis above, the overall structure of the end effector is defined, as shown in Fig. 1, which is more complex because of the integration of riveting process.

The basic processing modules for drilling are as follows:

(1) Pressure foot: Clamp the stacks with a suitable force to preclude the layer gap to further eliminate the formation of burrs between layers, during the drilling and riveting processes. Increase the system rigidity and stability in the meantime. The clamp force should be steplessly adjusted from 0 to 2 000 N, according to the studied processing mechanisms.

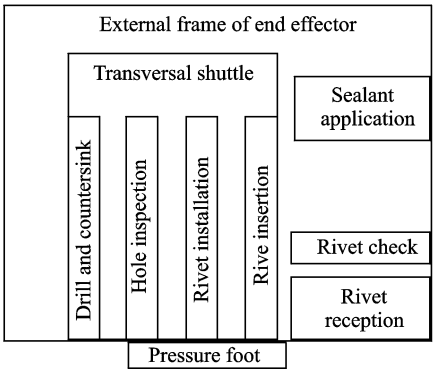

Fig. 1 Overall structure of the end effector

(2) Drilling and countersinking module: Carry out a one-step drilling and countersinking process on single or laminated aluminum and CFRP materials via a special drill with chamfer, which is designed to limit exit burrs and fiber breakout. The rotary speed of the spindle could be steplessly adjusted from 0 to 18 000 r/min, and the feed speed of the spindle could also be steplessly adjusted from 0 to 0.08 mm/(r·min^{-1}), in order to satisfy the different processing parameters for different materials. The diameter precision of a hole should be maintained within H8, and the countersink depth tolerance is required within ±0.01 mm.

(3) Hole inspection module: Measure the hole diameter, countersink depth and stack thickness via a high precision probe[14]. Gather the necessary information for verifying or selecting a specific rivet for each hole.

Additional modules for riveting:

(1) Rivet reception and geometry check module: Receive the rivet blown from the automatic rivet feed equipment and check the diameter and length of it.

(2) Sealant application and rivet insertion module: Apply sealant to the rivet and insert it in a pre-drilled hole.

(3) Riveting module: Blind rivet installation.

Each processing module of the end effector should work individually and harmoniously with

others, and the standard processing flow of the end effector is illustrated in Fig. 2.

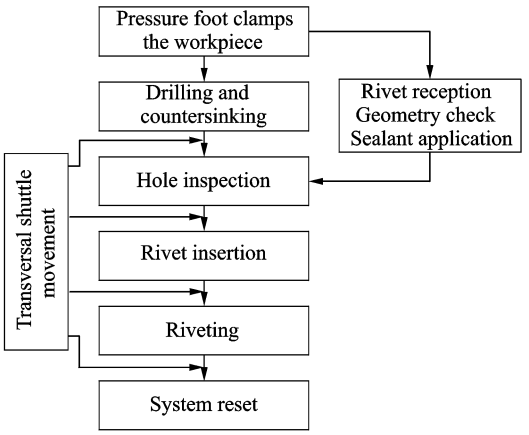

Fig. 2 Standard process flow of the end effector

2 Design of Main Functional Modules

2.1 Drilling and countersinking module

This is a critical module for the whole project, since the precision of the drilled hole will directly influence the quality of the joints finally riveted. This module mainly consists of an electrospindle, a special drill with chamfer and a servo linear unit, as shown in Fig. 3. The electrospindle (Renaud 430-120380-HSK40E) with a maximum speed of 19 700 r/min, controlled by a frequency inverter (EMERSON Unidrive SP3), has the racial and axial bouncing within 3 μm, which provides the basic hardware support for ensuring the diameter precision. And the drilling and countersink movement is precisely promoted by a servo motor (Siemens 1FT7044) controlled by the Siemens S120 motion control system with a special source of two encoder mode, one encoder presents inside the servo motor and the other, a length gauges (Heidenhain ST1278, accuracy of ±0.2 μm), fixed directly in the spindle base. The two-encoder system allows the control of the countersink depth to a precision within ±0.01 mm.

2.2 Rivet reception and geometry check module

This effector could rivet up to seven types of rivets on the product, the diameter of which may vary from 3.3 mm to 4.2 mm, and the length va-

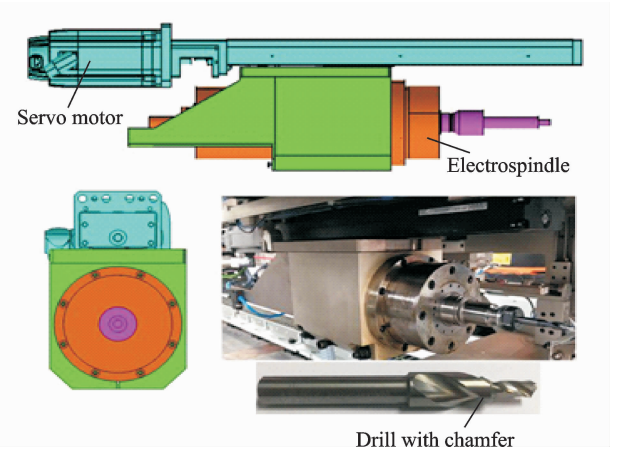

Fig. 3 Drilling and countersink module

ry from 32.18 mm to 38.31 mm. To automate the riveting process, it is not realistic to feed the rivets manually, so an automatic rivet feed equipment is developed, as shown in Fig. 4.

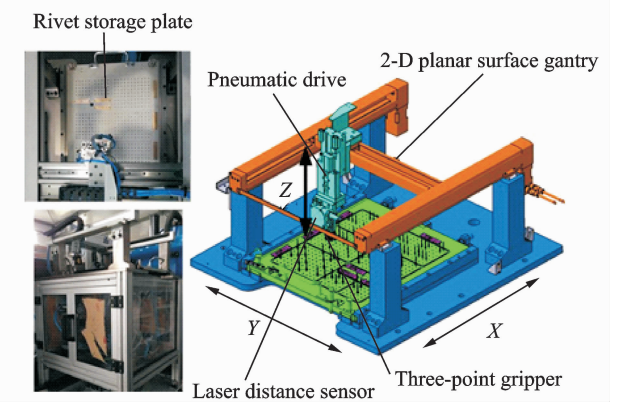

Fig. 4 Automatic rivet feeding equipment

A three-point gripper used to grasp the rivet and a laser distance sensor (BALLUFF BOD26K) used to primarily check the rivet length are mounted on a pneumatic drive that enables motion along Z axis, besides, all of them are installed on a 2-D planar surface gantry (FESTO EXCM-30) that allows for motions along X/Y axis. The rivets are previously inserted in the storage plate waiting to be selected by the gantry, checked by the sensors and grasped by the gripper, and finally blown to the rivet reception and geometry check module on the end effector.

In the rivet reception and geometry check module, the rivet reception is carried out by several pneumatic components and the geometry check is realized by two laser distance sensors, as

shown in Fig. 5. A parallel gripper is mounted on a pneumatic drive, which can move forward and backward along the Z axis. When a rivet reaches the outlet, the gripper will move forward and grasp it. After the gripper moves back, the first laser sensor (BALLUFF BOD26K) will measure the distance between itself and the gripper, then we could use this distance feedback to decide the rivet diameter. After that, the length check mechanism will move downward along Y axis also via a pneumatic drive, then the gripper will move forward again to insert the rivet into this mechanism to push a rod, inside this mechanism, backward, and the second senor (BALLUFF BOD18KF) will measure the distance between itself and the end of the rod to double check the exact length of the rivet. After geometry check, the gripper will move rightward along X axis, via another pneumatic drive, and insert the rivet in a three-point gripper. It should be noted that, the diameter and length feedback of different rivet types will be obtained previously in teach-in mode, and if the rivet type is wrong, a relevant disposal procedure will be carried out by the sealant application and rivet insertion module, as shown in Fig. 5.

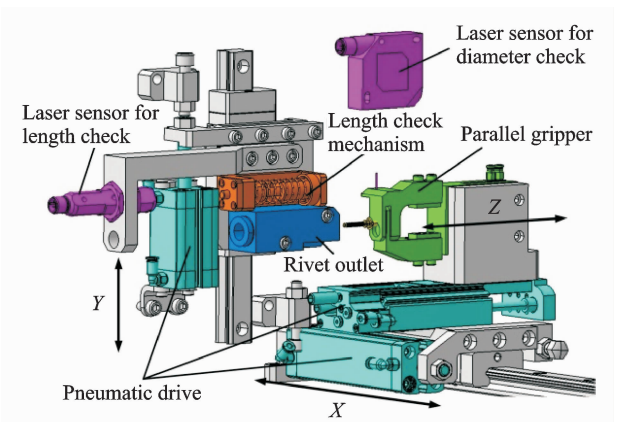

Fig. 5 Rivet reception and geometry check module

2.3 Sealant application and rivet insert module

This module mainly consists of a sealant application unit and a rivet insertion unit, which is aimed to simulate a manual procedure to apply sealant to the rivet and insert it in a pre-drilled hole. In the sealant application unit, a container is used to store the sealant, which also comprises a piece of sponge used for wiping away the excess sealant on the rivet. A color sensor (BALLUFF BFS 27K) is fastened beside the container to verify the quality of sealant application. In addition, both of them are mounted on a linear unit promoted by a servo motor, whose linear displacement depends on the amount of the sealant remaining in the container. In the rivet insertion unit, a three-point gripper is mounted on a rotary pneumatic drive, which enables it rotate clockwise and counterclockwise to facilitate sealant application, and both of them are installed on a slide that promoted by a pneumatic drive to execute rivet insertion. Besides, two small air cylinders are included in this unit to work as mechanical limit, which enable the slide stop at different positions to execute sealant wiping and wrong rivet disposal procedures. The realization of the sealant application and rivet insertion is carried out by the cooperation of each unit, as shown in Fig. 6.

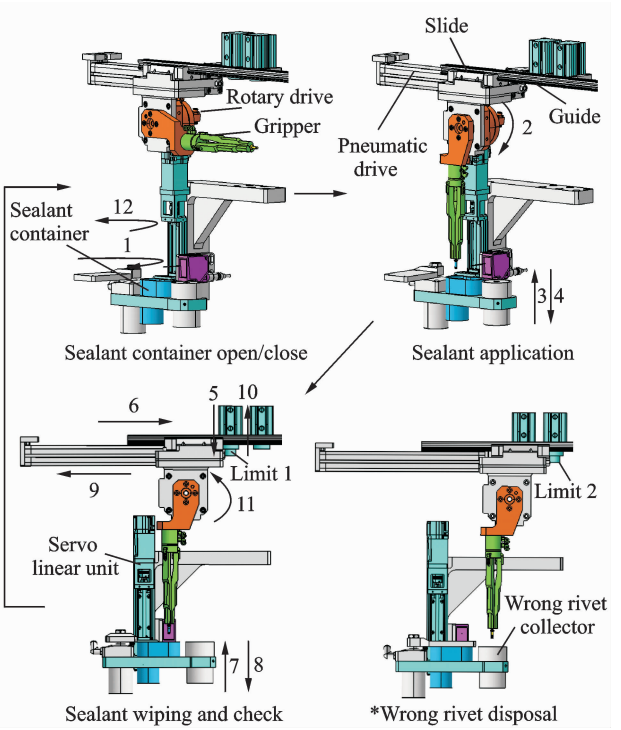

Fig. 6 Sealant application procedures

2.4 Riveting module

A riveting tool (CHERRY 704B-SR) with a pro-longed pulling head has been remodeled for this module, as shown in Fig. 7. This tool mainly consists of a riveting head, a power unit and the relevant pipelines between them. To integrate

this tool on the end effector, a mounting base has been designed to fit the riveting head, which has the relevant interface for the pipelines. The riveting head and the mounting base are both fastened on a slider, which is promoted by a pneumatic drive to hold the rivet that is pre-inserted in the hole. And the power unit is mounted on the side of the end effector, a mounting base with relevant interface for the pipelines should also be designed to fit this unit and an additional air cylinder is installed to actuate the riveting process.

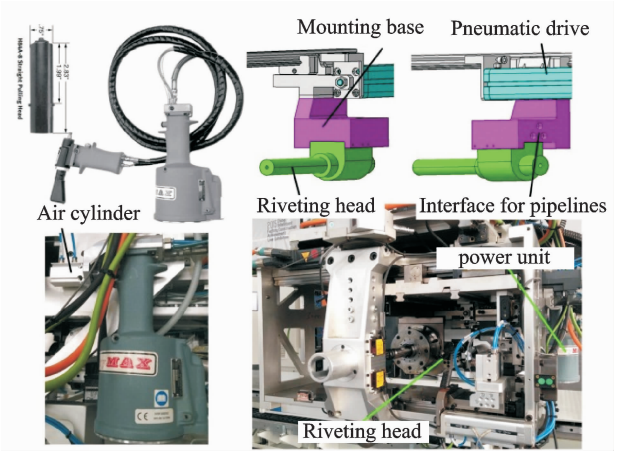

Fig. 7 Riveting module

After the schematic design of the effector and elaborate designs of each mainly functional module, the end effector would fulfill the basic functionality and provide the primary hardware support for the satisfactions of the stringent processing requirements. But during the real application, there will be many varying factors, which could not be counteracted merely by the hardware, so other measures have to be taken.

3 Online Detection and Adjustment

Usually, the positioning accuracy of the joint is really strict in aircraft assembly, within ± 0.5 mm, which could be guaranteed by the increased absolute positioning accuracy of robot and reference detection. Although the position of a target hole could be directly extracted from the 3-D model, there exist some position-pose deviations between the actual product and the nominal one, so we could not use the NC codes generated by offline programming directly. Besides, since the quality of a drilled hole will directly determine the quality of a joint riveted, the perpendicular accuracy of a hole is usually required within $0.5°$, which will neither be totally satisfied according to the NC codes, due to the shape deviations between the actual product and the nominal one. Then, to better guarantee the quality of the hole drilled and joints riveted, several online detection and adjustment measures have also been applied to this end effector:

(1) Reference detection: Retrieve the actual positions of the reference holes or joints, which are processed with high precision, to obtain the actual position and pose of the product. Then calculate the transformation relationships between the actual product and the nominal one to finally get NC codes revised.

(2) Normal calibration: Calculate the actual normal vector of the target drill surface to measure the deviations between itself and the current tool centerline. Then further figure out the actual pose that the robot needs to adjust to, and finally get the perpendicular accuracy satisfied by the adjustment of the robot.

3.1 Reference detection

The reference detection is mainly carried out by a 2-D laser-profile scanner (MICRO EPSILON scanCONTROL 2900-25) mounted on a servo linear unit, which helps to cover the scanning range, as shown in Fig. 8. The 2-D laser-profile sensor could get the X and Z coordinates of the points that it beamed on the subject, and the Y coordinates could be gained by the linear unit via grating scale. After scanning, we extract the points on the rim of the hole to define the reference plane and the \$Reference (Reference plane coordinates), as well as the relationship between itself and the \$Sensor (Sensor coordinates), then we could obtain the exact coordinates of the hole center under the \$Sensor. After scanning at least three reference holes or tag rivets, we could use the center coordinates of them to obtain the actual product position/orientation via coordinate

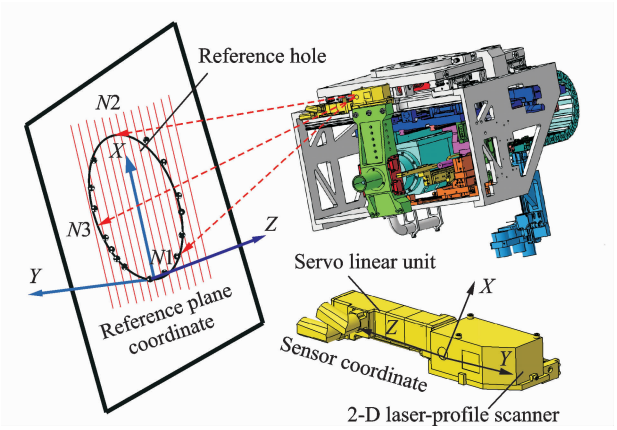

Fig. 8 Reference detection module

transformation and finally get the NC codes revised.

The working procedures are illustrated as follows:

(1) Recognize and extract the points on the rim of the reference hole by monitoring the sudden change in Z direction, and the points could be defined as $\boldsymbol{N}_i(x_k^t, y^t, z_k^t)$, x_k^t and z_k^t are obtained by the 2-D scanner, which belong to the number k point in the beam at time t. y^t is the absolute displacements of the linear unit at time t.

(2) Define the $ Reference by three randomly selected rim points, which are named as $\boldsymbol{N}_1(x'_1, y'_1, z'_1)$, $\boldsymbol{N}_2$ (x'_x, y'_x, z'_x), $\boldsymbol{N}_3(x'_3, y'_3, z'_3)$, and

$$\boldsymbol{n} = \boldsymbol{N}_1\boldsymbol{N}_2 \times \boldsymbol{N}_2\boldsymbol{N}_3 \tag{1}$$

where $\boldsymbol{n}$ is the normal of the reference plane and the $ Reference could be defined as

$$\begin{cases} \boldsymbol{x} = \boldsymbol{N}_1\boldsymbol{N}_2 / |\boldsymbol{N}_1\boldsymbol{N}_2| \\ \boldsymbol{y} = \boldsymbol{N}_1\boldsymbol{N}_2 \times \boldsymbol{n} / |\boldsymbol{N}_1\boldsymbol{N}_2 \times \boldsymbol{n}| \\ \boldsymbol{z} = \boldsymbol{n} / |\boldsymbol{n}| \end{cases} \tag{2}$$

The description of the $ Reference under the $ Sensor will be

$${}^{\text{Sensor}}_{\text{Reference}}\boldsymbol{T} = \begin{vmatrix} \boldsymbol{x}^{\mathrm{T}} & \boldsymbol{y}^{\mathrm{T}} & \boldsymbol{z}^{\mathrm{T}} & \boldsymbol{N}_1 \\ \boldsymbol{0} & \boldsymbol{0} & \boldsymbol{0} & \boldsymbol{1} \end{vmatrix} \tag{3}$$

(3) Transform all the rim points $\boldsymbol{N}_i$ to the newly defined $ Reference

$$\boldsymbol{N}_i^{\text{Reference}} = {}^{\text{Sensor}}_{\text{Reference}}\boldsymbol{T}^{-1} \times \boldsymbol{N}_i \tag{4}$$

(4) Use $\boldsymbol{N}_i^{\text{Reference}}$ to fit a circle in the reference plane, via the least square method, and transform the center coordinates of the fitted circle, $(a, b, 0)$, back to the $ Sensor, shown as

$$\begin{bmatrix} x'_c \\ y'_c \\ z'_c \\ 1 \end{bmatrix} = {}^{\text{Sensor}}_{\text{Reference}}\boldsymbol{T} \begin{bmatrix} a \\ b \\ 0 \\ 1 \end{bmatrix} \tag{5}$$

where (x'_c, y'_c, z'_c) is the actual position of the reference hole center under the $ Sensor, and (x, y, z) is the nominal position of the reference hole center under the $ World (World coordinates), then we will get

$${}^{\text{World}}_{\text{Sensor}}\boldsymbol{T} \times \begin{bmatrix} x'_c \\ y'_c \\ z'_c \\ 1 \end{bmatrix} = {}^{\text{Actural}}_{\text{Norminal}}\boldsymbol{T} \begin{bmatrix} x \\ y \\ z \\ 1 \end{bmatrix} \tag{6}$$

(5) ${}^{\text{World}}_{\text{Sensor}}\boldsymbol{T}$ is known beforehand, and use at least three reference holes or joints to calculate the ${}^{\text{Actural}}_{\text{Norminal}}\boldsymbol{T}$, and finally get the NC codes revised as

$$P_{\text{NCrevised}} = {}^{\text{Actural}}_{\text{Norminal}}\boldsymbol{T} \times P_{\text{NC}} \tag{7}$$

where P_{NC} is the nominal target position in the NC codes generated by offline programming, and $P_{\text{NCrevised}}$ is the actual target position, which will be used in the actual processing procedures.

3.2 Normal calibration

The feedback from four photoelectric distance sensors (Baumer OADM 12I6460/S35A), which are mounted on the either sides of the pressure foot, as shown in Fig. 9, is used as the reference for normal calibration. The mounting positions of the sensors, S_1, S_2, S_3, S_4, must be in the same plane and should be satisfied as $|\boldsymbol{S}_1\boldsymbol{S}_4| = |\boldsymbol{S}_4\boldsymbol{S}_2| = |\boldsymbol{S}_2\boldsymbol{S}_3| = |\boldsymbol{S}_3\boldsymbol{S}_1|$, $|\boldsymbol{S}_1\boldsymbol{S}_2| = |\boldsymbol{S}_3\boldsymbol{S}_4| = l$, $\boldsymbol{S}_1\boldsymbol{S}_2$ and $\boldsymbol{S}_3\boldsymbol{S}_4$ are defined as the Z axis and Y axis of the $ Tool (Tool coordinates) separately. When the end effector starts the processing cycle at a required position on the workpiece, the robot will locate it at a suitable position with a proper pose according to the revised NC codes, at which the pressure foot adjoins the workpiece and the tool centerline almost perpendicular to the surface. After that, adopt a calibration strategy introduced by Zhou[15], applying the distance feedbacks from the sensors, $\boldsymbol{S}_1\boldsymbol{Q}_1, \boldsymbol{S}_2\boldsymbol{Q}_2, \boldsymbol{S}_3\boldsymbol{Q}_3, \boldsymbol{S}_4\boldsymbol{Q}_4$, to the relevant algorithm to calculate the actual deviations between the tool centerline and the

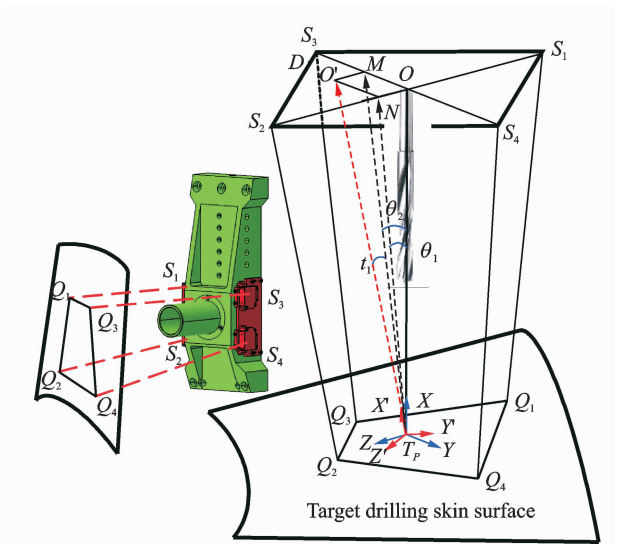

Fig. 9 Normal calibration module

normal of the target surface, then finally figure out the pose that the robot needs to adjust to.

In Fig. 9, T_P-XYZ is the $ Tool before normal calibration, and T_P-$X'Y'Z'$ is the one after adjustment, T_P is the virtual tool center point, which remains still during the calibration. $\boldsymbol{T_pO}$ is the tool centerline vector, $\boldsymbol{T_pO'}$ is the normal of the target drilling skin surface, $\boldsymbol{T_pM}$ and $\boldsymbol{T_pN}$ are the projections of $\boldsymbol{T_pO'}$ in the plane YT_PZ and plane XT_PZ, separately. Define the angle between the X axis and $\boldsymbol{T_pN}$ as θ_1, the angle between the X axis and $\boldsymbol{T_pM}$ as θ_2, the angle between $\boldsymbol{T_pM}$ and $\boldsymbol{T_pO'}$ as t_1, and then from the geometry relationships, we can get

$$t_1 = \arctan(\tan\theta_1 \times \cos\theta_2) \tag{8}$$

where θ_1 and θ_2 could be calculated from the distance feedbacks, according to the geometry relationships illustrated in Fig. 10, shown as

$$\theta_1 = \arctan[(|\boldsymbol{S_2Q_2}| - |\boldsymbol{S_1Q_1}|)/l] \tag{9}$$

$$\theta_2 = \arctan[(|\boldsymbol{S_3Q_3}| - |\boldsymbol{S_4Q_4}|)/l] \tag{10}$$

Presume the current position and pose of the robotis is (x, y, z, a, b, c), which defines the transformation from $ Base (Base coordinates) to T_P-XYZ, and assume the position and pose of the robot after the adjustment is (x, y, z, a', b', c'), which defines the transformation from $ Base to T_P-$X'Y'Z'$, then we will have

$$^{\$\,\mathrm{Base}}_{T_p\text{-}XYZ}\boldsymbol{T} = \mathrm{Trans}(x,y,z)\cdot\mathrm{Rot}(z,a)\cdot \mathrm{Rot}(y,b)\cdot\mathrm{Rot}(x,c) \tag{11}$$

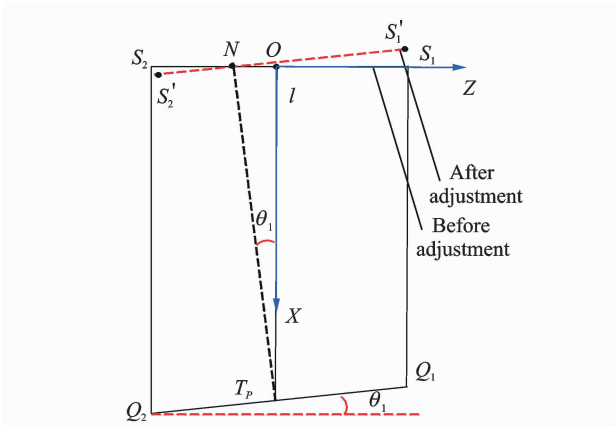

Fig. 10 Relationships between θ_1 and S_1Q_1, S_2Q_2 in plane XT_PZ

$$^{\$\,\mathrm{Base}}_{T_p\text{-}X'Y'Z'}\boldsymbol{T} = \mathrm{Trans}(x,y,z)\cdot\mathrm{Rot}(z,a')\cdot \mathrm{Rot}(y,b')\cdot\mathrm{Rot}(x,c') \tag{12}$$

According to the geometry relationships illustrated in Fig. 9, T_P-$X'Y'Z'$ could be transformed from T_P-XYZ by the following steps:

(1) T_P-XYZ rotates angle θ_2 around its original Z axis.

(2) T_P-XYZ rotates angle t_1 around the current Y axis, which is newly transformed from step (1).

Then the transformation between T_P-XYZ and T_P-$X'Y'Z'$ will be

$$^{T_p\text{-}XYZ}_{T_p\text{-}X'Y'Z'}\boldsymbol{T} = \mathrm{Trans}(0,0,0)\cdot\mathrm{Rot}(z,\theta_2)\cdot \mathrm{Rot}(y,t_1)\cdot\mathrm{Rot}(x,0) \tag{13}$$

According to Eqs. (11)—(13), we will further get

$$^{\$\,\mathrm{Base}}_{T_p\text{-}X'Y'Z'}\boldsymbol{T} = {}^{\$\,\mathrm{Base}}_{T_p\text{-}XYZ}\boldsymbol{T}\cdot {}^{T_p\text{-}XYZ}_{T_p\text{-}X'Y'Z'}\boldsymbol{T} \tag{14}$$

Integrate Eqs. (8)—(10), and we could finally figure out (a', b', c'), which will define the exact pose that the robot needs to adjust to.

4 Tests

An end effector is finally manufactured and assembled according to the designs mentioned above, and a platform is built, as shown in Fig. 11, which includes KR500 KUKA robot, end effector, experimental assembly fixture and laser tracker, etc. In the field application, we have two kinds of test coupons made of different materials, aluminum (7075) and CFRP (CCF300), but with

the same dimensions, 250 mm×80 mm×3 mm. Holes are drilled and countersank on aluminum coupons, CFRP coupons, and CFRP and aluminum laminated coupons, with relevant processing parameters by a same drill, whose diameter is 4.16 mm. It should be noted that parts of these coupons are processed in a "drill-only" mode, without countersank, for convenience to measure the dimensions and exact position of each hole, by the trilinear coordinates measuring instrument.

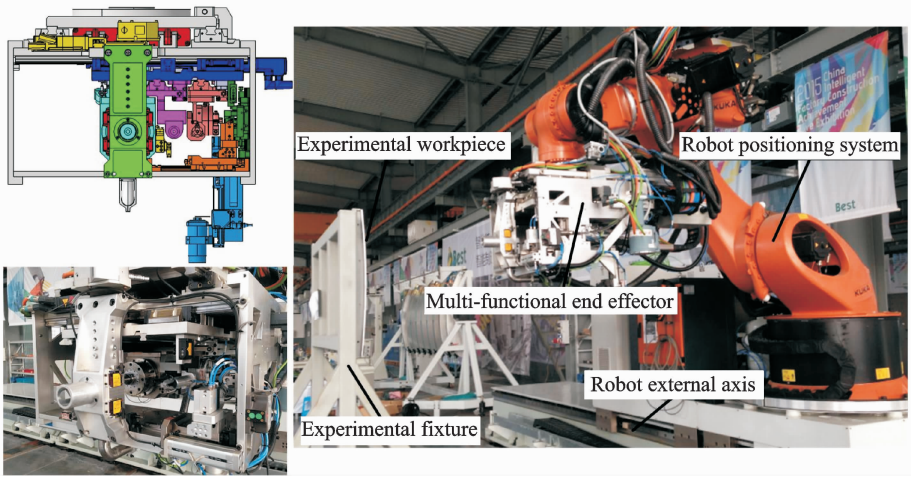

Fig. 11 Field application hardware

Besides, additional CFRP and aluminum laminated coupons, each coupon with a dimension of 80 mm×40 mm×3 mm, are drilled and further jointed together by a single Cherry CR7771S-5-3 blind rivet to test the shearing strength and tensile strength for a single joint, and the tests are carried out by the stretch test machine.

The measuring results show that this multi-functional end effector is capable of producing each hole to a positioning precision within ±0.5 mm, a perpendicular accuracy within 0.3°, a diameter tolerance of H8, and a countersink depth tolerance of ±0.01 mm. And it could drill and rivet up to three joints per minute, with an average shearing strength of 2 080 N and an average tensile strength of 950 N for a Cherry CR7771S-5-3 blind rivet.

5 Conclusions

(1) A multi-functional end effector is developed to automate the drilling and riveting processes for CFRP/aluminum components in robotic aircraft assembly. Different processing modules on the mul-tifunctional end effector are designed to realize this "one-up" drilling and riveting assembly goal. Besides, several online detection and adjustment measures are applied to this end effector to better guarantee the quality of the hole drilled and joints riveted.

(2) The field application shows that, the skematic design and overall workflow of this end effector are valid, different modules could work harmoniously and correctly, and this end effector is capable of producing each hole within the requied precision and riveting each joint with acceptable shearing and tensile strength.

Acknowledgements

The work was supported by the National Natural Science Foundations of China (Nos. 5157051626, 51475225).

References:

[1] XU G K. Automatic assembly technology for large ai-rcraft [J]. Acta Aeronoutica et Astronautica Sinica,2008, 29(3): 734-740.

[2] SUMMERS M. Robot capability test and development of industrial robot positioning system for the aerospace industry[J]. SAE Trans, 2005, 114(1): 1108-1108.

[3] BI S, LIANG J. Robotic drilling system for titanium structures [J]. Int J Adv Manuf Technol, 2011, 54 (5/6/7/8): 767-774.

[4] DEVLIEG R. Expanding the use of robotics in air-

frame assembly via accurate robot technology [J]. SAE Int J Aerosp, 2010, 3(1): 198-203.

[5] DEVLIEG R, SZALLAY T. Applied accurate robotic drilling for aircraftfuselage [J]. SAE Int J Aerosp,2010, 3(1): 180-186.

[6] QU W W, DONG H Y, KE Y L. Pose accuracy compensation technology in robot-aided aircraft assembly drilling process [J]. Acta Aeronautica et Astronautica Sinica, 2011, 32(10): 1951-1960.

[7] OLSSON T, ROBERTSSON A, JOHANSSON R. Flexible force control for accurate low-cost robot drilling [C]// 2007 IEEE International Conference on Robotics and Automation. [S. l.]: IEEE, 2007: 4770-4775.

[8] DEVLIEG R, SITTON K, FEIKERT E, et al. ONCE (ONe-sided cell end effector) robotic drilling system [C]//Proceedings of the 2002 SAE Aerospace Automated Fastening Conference and Exhibition. Warrendale, USA:[s. n.], 2002: 975-982 .

[9] DEVLIEG R. Robotic trailing edge flap drilling system [C]// Aerospce Technology Conference and Exhibition. [S. l]:SAE, 2009: 653-660.

[10] DEVLIEG R, FEIKERT E. One-up assembly with robots [C]//SAE Aerospace Manufacturing and Automated Fastening Conference and Exhibition. [S. l.]:SAE, 2008: 543-549.

[11] MEHLENHOFF T, VOGL S. Automated fastening of aircraft cargo door structures with a standard articulating robot system [C]//SAE Aerospce Technology Conference and Exhibition. [S. l.]: SAE, 2009: 442-448.

[12] BI Y B, LI Y C, GU J W, et al. Robotic automatic drilling system [J]. Journal of Zhejiang University (Engineering Science), 2014, 48 (8): 1427-1433.

[13] ZHANG J, WANG C W, LIAN P. Traveling robot automatic drilling and riveting technology and equipment [J]. Manufacturing Automation, 2015, 37 (5): 125-128.

[14] SMITH J, KOCHHAR-LINDGREN D. Integrated hole and countersink inspection of aircraft components [C]// SAE Aero Tech Congress and Exhibition. [S. l.]:SAE, 2013: 351-358.

[15] TIAN W, ZHOU W X, Zhou W, et al. Auto-normalization algorithm for robotic precision drilling system in air-craft component assembly [J]. Chinese Journal of Aeronautics, 2013, 26(2):498-500.

Dr. **Zhang Lin** was born in 1975. He is currently an assistant professor in Nanjing University of Aeronautics and Astronautics (NUAA). His research interests include aircraft automated assembly, CNC technology and precision machining technology. From 2004 to 2008, he studied for Ph. D. in NUAA. Since 2008, he has worked in NUAA. He worked as a visiting scholar in Cranfield University of UK from 2015 to 2016.

Prof. **Tian Wei** received his Ph. D. degree in Mechanical Manufacture and Automation from Nanjing University of Science and Technology in 2007. He currently works in Nanjing University of Aeronautics and Astronautics and his research interest focuses on aircraft intelligent assembly technology.

Mr. **Li Dawei** received M. S. degree in Manufacturing Engineering of Aerospace from Nanjing University of Aeronautics and Astronautics in 2017. He currently works in 206 Institutes of the Second Institute of Space Science and Technology.

Mr. **Hong Peng** received M. S. degree in Manufacturing Engineering of Aerospace from Nanjing University of Aeronautics and Astronautics in 2016. He currently works in Nanjing Chenguang Group Co. Ltd.

Mr. **Li Zhenyu** received M. S. degree in Manufacturing Engineering of Aerospace from Nanjing University of Aeronautics and Astronautics in 2016. He currently works in Envision Energy Technology (Shanghai) Co. Ltd.

Ms. **Zhou Weixue** received M. S. degree in Manufacturing Engineering of Aerospace from Nanjing University of Aeronautics and Astronautics in 2013. She currently works in Beijing Aerospace Long March Aircraft Research Institute.

Prof. **Liao Wenhe** is a professor in School of Mechanical Engineering, Nanjing University of Science and Technology. His research interest focuses on microsatellite, aircraft automated assembly and 3D printing.

(Production Editor: Sun Jing)